https://doi.org/10.5194/acp-2021-325
Preprint. Discussion started: 9 July 2021


Atmospheric Chemistry and Physics Discussions
Open Access
EGU

# Large eddy simulation of boundary-layer turbulence over the heterogeneous surface in the Source Region of the Yellow River

Yunshuai ZHANG[a], Qian HUANG[a,*], Yaoming MA[a,b,c,d], Jiali LUO[a], Chan WANG[e], Zhaoguo LI[e], and Yan CHOU[a]

[a] *Key Laboratory for Semi-Arid Climate Change of the Ministry of Education, College of Atmospheric Sciences, Lanzhou University, Lanzhou* 730000*, China*
[b] *Key Laboratory of Tibetan Environment Changes and Land Surface Processes, Institute of Tibetan Plateau Research, Chinese Academy of Sciences, Beijing* 100101*, China*
[c] *University of Chinese Academy of Sciences, Beijing* 100049*, China*
[d] *CAS Center for Excellence in Tibetan Plateau Earth Sciences, Chinese Academy of Sciences, Beijing* 100101*, China*
[e] *Key Laboratory of Land Surface Process and Climate Change in Cold and Arid Regions, Northwest Institute of Eco-Environment and Resources, Chinese Academy of Sciences, Lanzhou* 730000*, China*

## Abstract

Lake breezes are proved by downdrafts and the divergence flows of zonal wind in the source region of the Yellow River (SRYR) in the daytime based on ERA-Interim reanalysis data. In order to depict the effect of the circulations induced by surface anomaly heating (patches) on the boundary-layer turbulence, the large eddy model was used to produce a set of 1D strip-like surface heat flux distributions based on observations, which obtained by a field campaign in the Ngoring Lake Basin in the summer of 2012. The simulations show that for the cases without ambient winds, patch-induced circulations (SCs) enhance the turbulent kinetic energy (TKE) and then modify the spatial distribution of TKE. Based on phase-averaged analysis, which

*Corresponding author.
E-mail address: huangq@lzu.edu.cn (Q. Huang).

https://doi.org/10.5194/acp-2021-325
Preprint. Discussion started: 9 July 2021


separates the attribution from the SCs and the background turbulence, the SCs contribute no more than 10% to the vertical turbulent intensity, but their contributions to the heat flux can be up to 80%. The lake patches produce consistent spatial distributions of wind speed and turbulent stress over the lake–land boundary, and the obvious change of turbulent momentum flux over the boundary of patches can not be neglected. In the entrainment layer, the convective rolls still persist under stronger geostrophic winds of 7–11 m $s^{-1}$. The increased downdrafts, which mainly occur over the lake patches and carry more warm, dry air down from the free atmosphere. In general, the SCs promote the growth of convective boundary layer, while the background flows inhibit it. The background winds also weaken the patch-induced turbulent intensity, heat flux, and convective intensity.

**Key word:** turbulence, heat flux, heterogeneously surface heating, background flows, phase-averaged analysis

# 1. Introduction

Turbulence in the planetary boundary layer (PBL), which is derived from surface heating and surface fraction, plays an important role in the exchange of heat, momentum, moisture, and chemical constituents between the surface and free atmosphere (Zhang et al., 2018). Previous studies on the turbulence and turbulent exchange over homogeneous surfaces based on Monin-Obukhov similarity theory were conducted before the 1990s (Sommeria and LeMone, 1978; Moeng, 1984). Turbulence over heterogeneous surfaces was investigated through field campaigns (Wang et al., 2016; Zhao et al., 2018) and numerical simulations (Shao et al., 2013;

Liu et al., 2011) in the past few decades, which has improved our understanding of the transfer and spatial and temporal variability of the turbulence. Thermal surface heterogeneity is a typical issue and leads to the formation of local/secondary circulations. Sea and lake breezes are a well-known example of flows that are generated by heterogeneous surface heating between the land and water (Crosman and Horel, 2012). Observations have also revealed the imbalance in the surface energy budget over heterogeneous surfaces (Foken et al. 2010; Xu et al., 2016). The most widely used eddy covariance (EC) system for a single site has been shown to underestimate the turbulent flux due to the large-eddy transport or secondary circulations not being captured (Foken et al., 2010; Xu et al., 2016). The simulation studies conducted by Zhou et al. (2018) and Frederik and Matthias (2018) showed that the flux induced by mesoscale or secondary circulations is the main reason for the energy imbalance. Moreover, the PBL parameterization schemes in the weather/climate model over a heterogeneous surface have been continuously improved until now (Avissar and Pielke, 1989; Shao et al., 2013). Different surface patterns such as mosaic (Avissar and Schmidt, 1998), chessboard (Liu et al., 2011; Shen et al., 2016), patchy-like (Zhou et al., 2018), and strip-like (Li et al., 2011; Wang et al., 2011) patterns have been utilized to simulate thermodynamic surface heterogeneity. These studies confirmed that the secondary circulation induced by the surface heterogeneity influences the PBL's properties and turbulent characteristics. In addition, several studies have examined the effects of surface heterogeneity on different levels of background winds (Shen and Leclerc, 1995) and the direction

https://doi.org/10.5194/acp-2021-325
Preprint. Discussion started: 9 July 2021


Atmospheric Chemistry and Physics Discussions
Open Access
EGU

relative to the orientation of the heterogeneity (Wang et al., 2011; Kang and Lenschow, 2014). However, the issues related to the effects of the surface heterogeneity in special areas still need to be explored.

The dynamic and thermodynamic influences of the Tibetan Plateau (TP) on the regional and global weather and climate systems are closely related to its PBL, and turbulence plays a significant role in the mass and energy exchange between the TP and the atmosphere (Chen et al., 2013; Chen et al., 2016). Different landscapes make up the heterogeneous land surface over the TP. As the Asian Water Tower, lakes are widely and densely distributed over the TP, which affects the overlying energy and mass transport through the lake-air turbulent heat flux. Biermann et al. (2014) and Wang et al. (2015) discovered that the turbulent flux of Lake Nam co, which is surrounded by wet grasslands, is actually very considerable but was often underestimated in the model. The Source Region of the Yellow River (SRYR) is located in the northeastern part of the TP and is known as the "water tower" of China because it contains 48 lakes. The Ngoring and Gyaring (Sisters) Lakes are two major lakes, and Ngoring Lake is the largest in the SRYR (Li et al., 2015; Wen et al., 2015). In addition to the lakes, the forests, alpine meadow, wetlands, rivers, and glaciers comprise the diverse underlying surfaces in the SRYR, with grassland accounting for about 80% of the area (Mudassar et al., 2018). Consequently, the SRYR is an ideal region for studying the turbulence over a heterogeneous land surface.

Observational studies have revealed that water vapor, heat, and energy exchange occur over alpine meadows/wetlands (Zheng et al., 2015; Jia et al., 2017) and lakes

https://doi.org/10.5194/acp-2021-325
Preprint. Discussion started: 9 July 2021



(Li et al., 2015; Wen et al., 2016), and models have been used to simulated the effects of the lakes on the cool and moist regional climate (Wen et al., 2015; Ao et al., 2018). However, the features of the boundary-layer turbulence over the heterogeneous underlying surfaces and the effects of thermodynamic surface heterogeneity on the turbulent flux in the SRYR remain unclear. Over the last few decades, the lakes have shrunk and the grasslands have degraded in the SRYR due to climate change and the excessive utilization of water resources (Brierley et al., 2016; Mudassar et al., 2018). It is essential to investigate the variation in the structure of boundary-layer and turbulent heat flux with changes in the surface's thermal properties and the background winds.

High resolution field measurements are extremely rare on the TP because of the harsh environmental conditions, so few observational studies on the turbulence characteristics and the turbulent heat flux have been conducted. Large eddy simulation (LES) has the unique advantage of being accurate and able to describe turbulence finely, and thus, it has been widely used to investigate the effects of surface heterogeneity on turbulence (Hadfield et al., 1991, 1992; Kang and Lenschow, 2014). However, little has been done to improve our understanding of how the surface heterogeneity affects the boundary-layer turbulence, and the contributions of the patch-induced motions to the turbulent flux and energy in the SRYR. Furthermore, modeling the turbulence over the heterogeneous surface in the SRYR can not only lay a basis for the analysis of the local energy and mass transport, but it can also provide a quantitative reference for improving the parameterization schemes over

https://doi.org/10.5194/acp-2021-325
Preprint. Discussion started: 9 July 2021



heterogeneous surfaces in weather and climate models.

In this study, we used LES to investigate the detailed turbulence characteristics in the SRYR. Our primary focus was the impacts of the surface heat flux anomalies on the turbulent kinetic energy (TKE), turbulent intensity, and turbulent flux. The turbulence characteristics and turbulent fluxes in the surface and the entrainment layers were investigated, too. This paper is arranged as follows Section 2 describes the model and data used in this study. Section 3 discusses the modeled results in detail, and section 4 provides a summary and discussion of our findings.

# 2 data and methods

## 2.1 Study area and observations

Ngoring Lake and Gyaring Lake (hereinafter referred to as the two lakes) are located in the SRYR and are surrounded by the alpine meadow. Their mean elevation is 4274 m above sea level. The study area is shown in fig.1. The turbulent flux and standard atmospheric variables were measured over the lake and grassland surface. The GPS radiosonde data from the field campaign on July 29, 2012, 30 m west of Lake Ngoring (near the gradient tower station, TS) and at Madoi station (MD) located 30 km the east of the lake (34.918° N, 98.216° E, 4279 m AMSL), as well as the eddy covariance data for Lake Station (LS) above the northwest of the lake (35.026° N, 97.652° E) and Grassland Station (GS) (34.913° N, 97.553° E) 1.5 km west of the lake shore were used. For further details on the field campaign and the quality control of the sounding and eddy covariance data, see Li et al. (2015) and Li et al. (2017). The synoptic background near the surface and at 500 hPa and the distribution of the

https://doi.org/10.5194/acp-2021-325
Preprint. Discussion started: 9 July 2021




wind components in the vertical and horizontal directions were investigated using the ERA-Interim Reanalysis Data with a 1° × 1° resolution collected at 12:30 LT and 18:30 LT (LT: local time, used in the whole study) on July 29, 2012, with a delimiting a range of 32° N–37° N, 95° E–100° E, including the two lakes area (34.8° N–35° N, 97° E–98° E) and the surrounding grassland.

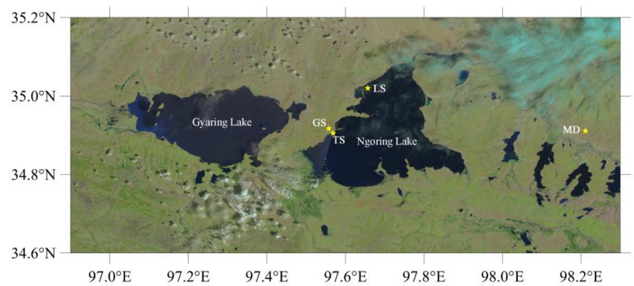


**Fig.1.** Map of the study area obtained using Landsat data, with the location of the observation stations marked by yellow stars. The turbulent fluxes were measured at LS and GS stations. The standard atmospheric variables were observed at the TS. MD is a fixed meteorological observatory of the China Meteorological Administration.

## 2.2 Methods

### 2.2.1 Simulations set-up over the heterogeneous underlying surface

The U.K. Met Office large eddy model (LEM) version 2.4 (Gray et al., 2001) was used in this paper. The LEM is a three-dimensional and non-hydrostatic numerical model, which can be used to simulate a wide range of turbulence-scale and cloud-scale problems with a high resolution. The domain size was 135 km × 30 km × 6 km with a horizontal grid-spacing of 200 m. A vertically stretched grid with a minimum spacing of 1.1 m was utilized in the surface layer and a maximum of 64.8 m above 2000 m. Periodic lateral boundary conditions were applied, with a rigid lid at the top of the model domain. To reduce the reflection of the internal gravity waves, a

https://doi.org/10.5194/acp-2021-325
Preprint. Discussion started: 9 July 2021




Newtonian damping layer was applied above 3500 m. The surface boundary conditions of the model were derived from the Monin-Obukhov similarity theory using the Businger-Dyer functions. The subgrid model used in the LEM was based on the Smagorinsky-Lilly approach (Brown et al., 1994). The potential temperature, wind (*u* and *v*), and relative humidity profiles obtained during the field campaign on July 29, 2012, were used to initialize the 3D runs. The LEM was driven by the time-varying sensible heat flux (SHF) and the latent heat flux (LHF) at the surface. The geostrophic wind shear was calculated using the ERA-Interim geostrophic wind at the surface and at 1500 m. The simulation time was 12 hours and the data were output every hour. In this study, twelve 3D runs with different surface heat fluxes under various ambient wind conditions were performed. Two of the runs were horizontally homogeneous with a uniform grass surface under the conditions of wind (HOMW) and no wind (HOM). The other cases were simulated with one (A1L) or two (A2L) lake patches in the middle of the model domain. The surface heat flux anomaly was applied over a 30 km wide strip (two strips for A2L) extending the entire 30 km width of the domain in the x-direction. Here the term heat flux refers to both the sensible and latent heat fluxes. This can be viewed as representing Ngoring Lake and Gyaring Lake in the SRYR. It should be noted that in this study the scale of the heterogeneity was large enough to enable the formation of small eddies over the lake patches that could coexist with the large-scale patch-induced circulations (Patton et al., 2005). Four simulations (A1L, A2L, A1LW, and A2LW) were initialized using the surface heat flux over the patch/patches measured at LS and the heat flux outside the patch/patches

https://doi.org/10.5194/acp-2021-325
Preprint. Discussion started: 9 July 2021




measured at GS. This means that the heat flux into the modeled atmosphere decreases as the number of patches increases. However, it is helpful to separate the effects of the total increase in heating from the effects of the localization of the heating when considering the consequences of an unresolved spatially changing heat flux for a global model. In order to keep the total heat flux in the modeled atmosphere constant, a "balanced" surface heat flux approach was used. Therefore, if the surface heat flux observed at the GS is denoted as FGS, and the heat fluxes over the patch and outside of the patch are denoted as FL and FG, respectively. FL and FG were calculated using the following equations:

$$FL = FGS \times (SL/ST) \quad (1)$$

$$FG = FGS \times (SG/ST) \quad (2)$$

where ST, SL, and SG are the squares of the model domain, the patch, and the outside of it, respectively. Another four simulations (A1L_C, A2L_C, A1LW_C, and A2LW_C) were performed using this balanced surface heat flux approach. The heterogeneous initial conditions were used in the surface heat flux anomaly simulations. The initial profiles over the patch/patches were derived using the data from TS station, and the data observed at the MD station used for the outside patch/patches. Various ambient wind conditions were also used for the surface heat flux anomaly runs. The parameters and the conditions of each run are listed in Table 1 for convenience. Sketches of the heterogeneous surface and of the surface heat fluxes over the lake patches and the outside patches for the unbalanced and balanced cases are depicted in fig. 2.

https://doi.org/10.5194/acp-2021-325
Preprint. Discussion started: 9 July 2021

Atmospheric Chemistry and Physics Discussions

The initial potential temperature and special humidity are shown in fig. 2h, and the horizontal components of the wind profiles and the geostrophic wind are shown in fig. 2g. A stable layer was found over the grass and a 200 m convective boundary layer (CBL) was found over the lake at 06:30 LT. The special humidity profiles show that the air tends to be moister over the lake (dash lines in fig. 2h). The study area is characterized by a considerable surface heat flux and high wind speeds in the daytime. The stronger initial velocity is from the GS, which recorded wind speeds of up to 10 m $s^{-1}$ below 500 m.

**Table 1**

Parameters for the 3D simulations.

| Name | Wind field | Surface heat flux (SHF and LHF) | Number of lake patches | Size of Lake patch (km) |
|---|---|---|---|---|
| HOM | without wind | FGS | 0 | - |
| HOMW | initial wind + geostrophic wind | FGS | 0 | - |
| A1L | without wind | lake patch: FLS (Heat flux that observed at LS); outside patch: FGS | 1 | 30 |
| A2L | without wind | lake patches: FLS (Heat flux that observed at LS); outside patches: FGS | 2 | 30 and 30 |
| A1LW | initial wind + geostrophic wind | Same as A1L | 1 | 30 |
| A2LW | initial wind + geostrophic wind | Same as A2L | 2 | 30 and 30 |

https://doi.org/10.5194/acp-2021-325
Preprint. Discussion started: 9 July 2021


Atmospheric Chemistry and Physics
Discussions

| | | | | |
|---|---|---|---|---|
| A1LNG | initial wind | Same as A1L | 1 | 30 |
| A2LNG | initial wind | Same as A2L | 2 | 30 and 30 |
| A1L_C | without wind | lake patch: (SL/ST) ×FGS =(30/135)× FGS; outside patch: (SG/ST)×FGS =(105/135)×FGS | 1 | 30 |
| A2L_C | without wind | lake patches: (SL/ST)×FGS =(30/135)×FGS; outside patches: (SG/ST)×FGS =(75/135)×FGS | 2 | 30 and 30 |
| A1LW_C | initial wind + geostrophic wind | Same as A1L_C | 1 | 30 |
| A2LW_C | initial wind + geostrophic wind | Same as A2L_C | 2 | 30 and 30 |

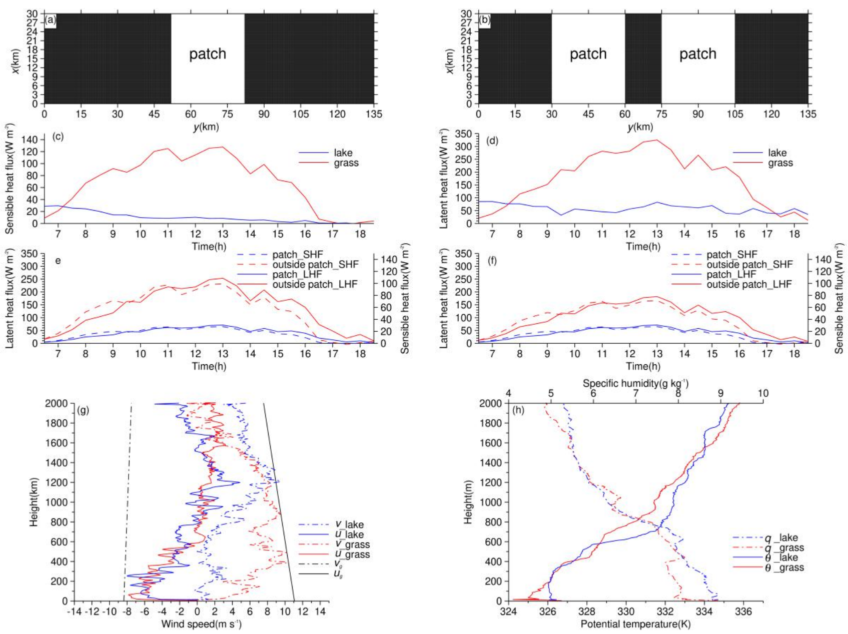

https://doi.org/10.5194/acp-2021-325
Preprint. Discussion started: 9 July 2021




**Fig. 2.** Sketch of the heterogeneous surface (a and b), (c and d) surface sensible heat flux and latent heat flux over the grassland (red line) and the lake (blue line) from observation. The SHF and the LHF for runs with (e) one and (f) two lake patches and a constant heat flux. Figures 2g and 2h show the initial profiles of the winds (solid lines for *u*, dash lines for *v*), potential temperature (solid lines), and special humidity (dash lines) over the lake patches (blue lines) and outside of the patches (red lines). The input geostrophic winds are also shown (black lines).

### 2.2.2 statistical analysis

According to turbulence theory, a physical quantity $\phi$ has two parts, i.e., the horizontal average $\langle\phi\rangle$ and the turbulent fluctuation $\phi'$, and

$$\phi = \langle\phi\rangle + \phi' \tag{3}$$

This equation usually works in cases with a homogeneous surface. The variances of velocity and the potential temperature variances ( $\sigma_v^2$ , $\sigma_w^2$ , $\sigma_\theta^2$ ) are calculated from $v'$, $w'$, and $\theta'$, respectively. For a heterogeneous surface, phase-averaged analysis helps separate the patch-induced circulations from the random turbulent motions. This method has been applied in studies of the one-dimension and two-dimension heterogeneities (Matthias et al., 2014; Kang and Lenschow, 2014; Shen et al., 2016) and complex and irregular heterogeneities (Maronga and Raasch, 2013). In this study, one-dimensional heterogeneous (in the *y* direction) simulations were performed for which $\phi$ can be decomposed into three parts:

$$\phi = \langle\phi\rangle + \phi_{hi} + \phi_s \tag{4}$$

Where $\langle\phi\rangle$ is the horizontal average; $\phi_{hi}$ is the heterogeneity-induced part which is the averaged $\phi$ across the domain in the *y* direction; and $\phi_s$ is from the background turbulence. The variances of velocity and the potential temperature induced by the heterogeneity ( $[\sigma_v^2]_{hi}$ , $[\sigma_w^2]_{hi}$ , $[\sigma_\theta^2]_{hi}$ ) are calculated from $v_{hi}$ , $w_{hi}$ , and $\theta_{hi}$ ,

https://doi.org/10.5194/acp-2021-325
Preprint. Discussion started: 9 July 2021



respectively.

Phase-averaged analysis was also used to obtain the patch-induced component of the turbulent fluxes. We multiplied $w$ and $\phi$ with both in the forms of Equation (4), and derived the total vertical transport of $\phi$:

$$\overline{\langle w\phi\rangle} = \overline{\langle w\rangle\langle\phi\rangle} + \langle w_{hi}\phi_{hi}\rangle + \overline{\langle w_s\phi_s\rangle} \quad (5)$$

Since the horizontal average vertical velocity $\langle w\rangle$ is approximately zero in the LES, the turbulent fluxes were divided into two parts: a patch-induced circulation induced part and a background turbulence induced part:

$$\overline{\langle w\phi\rangle} = \langle w_{hi}\phi_{hi}\rangle + \overline{\langle w_s\phi_s\rangle} \quad (6)$$

Moreover, the total kinetic energy $e$ can be written as two parts, $e_{hi}$ and $e_s$, which represent the contributions from the patch-induced and background turbulence:

$$e = e_{hi} + e_s \quad (7)$$

$$e_{hi} = \left(\langle u_{hi}{}^2\rangle + \langle v_{hi}{}^2\rangle + \langle w_{hi}{}^2\rangle\right)/2 \quad (8)$$

$$e_s = \left(\langle u_s{}^2\rangle + \langle v_s{}^2\rangle + \langle w_s{}^2\rangle\right)/2 \quad (9)$$

# 3. Results

## 3.1. Synoptic background and wind components' distribution

In order to investigate the existence of a daytime lake breeze (the divergent flows over the lake surface and the downdrafts overlying it) using the ERA-Interim reanalysis data for the two lakes area (34.8° N–35° N, 97° E–98° E; blue box in fig. 3), the wind field, temperature field, and geopotential height field at the surface (600 hPa, ~4200 m) and at 500 hPa (~5500 m) at 12:30 LT and 18:30 LT on July 29, 2012, were analyzed. A cyclone controlled the entire region above the surface at 12:30 LT (Fig. 3a)

https://doi.org/10.5194/acp-2021-325
Preprint. Discussion started: 9 July 2021

Atmospheric Chemistry and Physics Discussions

and divergent flow occurred at 500 hPa at 18:30 LT (Fig. 3b). The vertical sections of the two wind components ( *u* and *w*) were also depicted to further ascertain the distribution of the wind field in the longitude and latitude directions. It should be noted that downdrafts are dominant below 500 hPa in the two lakes area during the day (Figs. 3c and 3d). As can be seen from fig. 3f, distinct divergent zonal wind (*u*) flows existed in the two lakes area at 18:30 LT. The wind speed derived from the GPS sounding at 12:30 LT is larger than that at 18:30 LT below 2 km (see fig. S1 in supplement), indicating that the larger background flows covered up the divergent wind flow at 12:30 LT. Evidently, it is difficult to directly observe the lake breeze circulation due to the synoptic background, but the downdrafts and the divergent zonal wind in the two lakes area demonstrate the existence of a lake breeze. In the following sections, the turbulence characteristics over the heterogeneous underlying surface are simulated and the effects of the patch-induced circulation are analyzed.

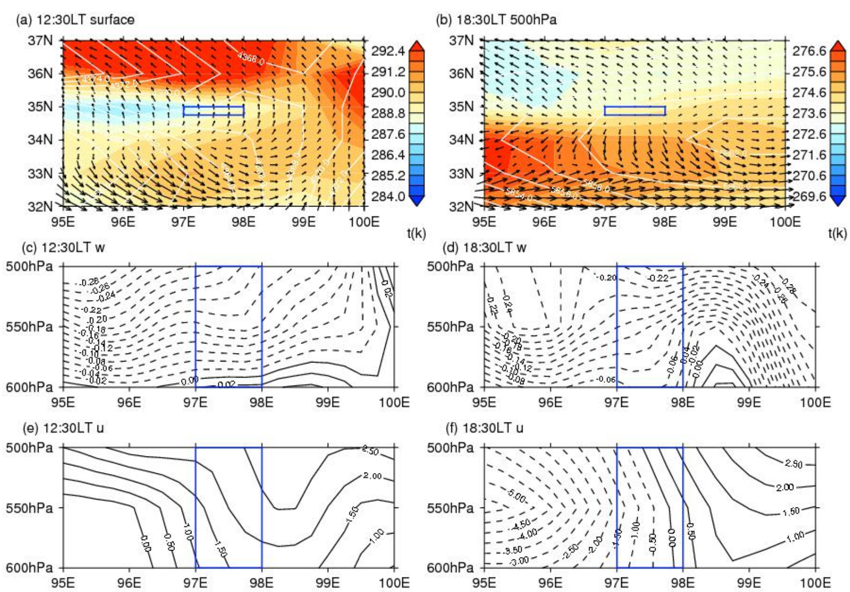

https://doi.org/10.5194/acp-2021-325
Preprint. Discussion started: 9 July 2021




**Fig. 3.** Synoptic background on July 29, 2012. Blue boxes represent the two lakes area. (a) and (b) show the wind field, temperature field, and geopotential height field at the surface (600 hPa, ~4200 m, 10 m wind field, 2 m temperature field; Fig. 3a) at 12:30 LT and at 500 hPa (~5500 m) at 18:30 LT (Fig. 3b). The vertical wind (*w*, figs. 3c and 3d) and the zonal wind (*u*, figs. 3e and 3f) below 500 hPa are also shown.

## 3.2 Effects of the underlying surfaces and background flows on the boundary-layer turbulence

### 3.2.1 Performance of the LEM and the height of the boundary layer over homogeneously heated and heterogeneously heated surfaces

In order to inspect the performance of the LEM over the heterogeneously heated surfaces, the simulated virtual potential temperature ( $\theta_v$ ) over the lake patch/patches and outside were compared with the observations. In addition, by keeping the total surface heat flux into the modeled domain constant, the profiles of the simulated virtual potential temperature over the homogeneous and heterogeneous surfaces were compared in order to investigate the effects of surface heterogeneity on the structure of the boundary layer. The profiles of the kinematic heat flux for all of the runs were used to determine the height of the boundary layer. Figures 4a and 4b compare the simulated profiles of the virtual potential temperature over and outside of the lake patch with the corresponding observations (solid lines) over the grassland and the lake surfaces at different times. In order to account for the effects of the unrepresented large-scale forcing, the simulated horizontally averaged potential temperature, water vapor mixing ratio, and horizontal wind (*u* and *v*) were relaxed to those observed using the radiosondes with at a 3 h interval during the simulation (Marsham et al.,

https://doi.org/10.5194/acp-2021-325
Preprint. Discussion started: 9 July 2021


Atmospheric Chemistry and Physics
Discussions

2008; Huang et al., 2009). The time series of the kinetic energy (see fig. S2 in supplement) indicates that the equilibration time of the model is approximately 3 hours.

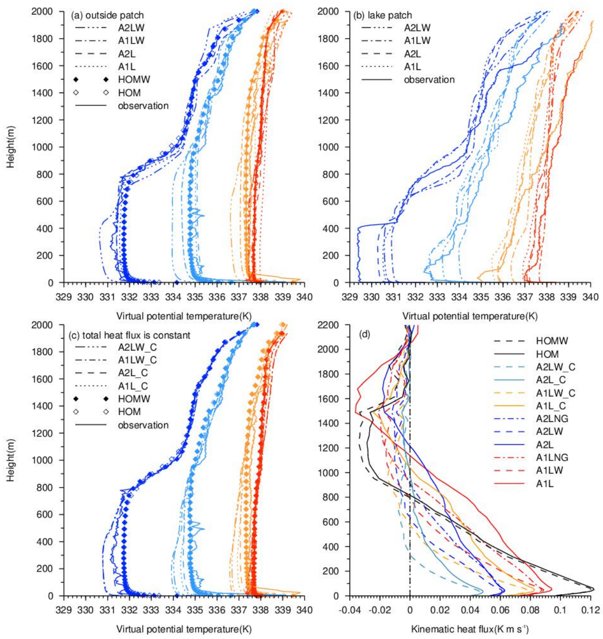


**Fig. 4.** The profile of the horizontal, averaged virtual potential temperature for the observations and all of the runs over the lake patches (a) and outside the of the (b) lake patches. (c) same as (a) except, for heterogeneous and homogeneous runs with constant surface heat fluxes. Legends for (a), (b), and (c): dark and light blue represent the results at 09:30 and 12:30, respectively, and the orange and red lines show the results at 15:30 and 18:30, respectively. (d) The kinematic heat fluxes for all of the runs.

The observation profiles (solid lines in fig. 4a) show that the depth of the convective boundary layer (CBL) over the grassland increases from 700 m at 09:30 to 1.1 km at 12:30 to 1.5 km at 15:30 to 1.9 km at 18:30. The inversion layer above the CBL is completely eroded by the turbulence after 12:30. The virtual potential temperature in the well-mixed CBL over the grassland increases approximately 7 K

https://doi.org/10.5194/acp-2021-325
Preprint. Discussion started: 9 July 2021



from 09:30 to 18:30. The CBL over the heterogeneous surfaces with background wind is cooler and shallower than that over the homogeneous surfaces. This may be because the air blowing from the lake patches cools the CBL of the outside patches that are downwind, which inhibits the development of the CBL. In addition, the model profiles of the virtual potential temperatures over the homogeneously heated and heterogeneously heated surfaces with no background wind have very similar structures and are close to the sounding profiles. This is similar to the modeling results of Liu et al. (2011). The observed virtual potential temperature over the lake surface (solid lines in fig. 4b) shows that the CBL changes to stable stratification as the radiation increases after sunrise, and the modeled $\theta_v$ over the patches is about 1.0 K warmer than the observed $\theta_v$. As in fig. 4a, fig. 4c also shows that the background wind over the heterogeneous surface inhibits the growth of the CBL.

In this study, according to Sullivan et al. (1998), the height of the boundary layer (*zi*) was determined using the minimum kinematic heat flux of the simulated results. As can be seen, the maximum surface heat fluxes were relatively large over the homogeneously heated surface, while smaller surface heat fluxes occurred for the case with two lake patches. Compared to the unbalanced cases (A1L, A1LW, A2L, and A2LW), less heat flux was introduced in the balanced cases (A1L_C, A1LW_C, A2L_C, and A2LW_C) and lower CBLs occurred, especially with a wind field (blue bars in fig. 5). The kinematic heat fluxes decreased to zero at higher altitude over the heterogeneously heated surface. When the height continues to rise, the region of negative heat flux is often called the entrainment layer, which is thicker in the cases

https://doi.org/10.5194/acp-2021-325
Preprint. Discussion started: 9 July 2021


Atmospheric Chemistry and Physics
Open Access
EGU
Discussions

with background wind. The heights of the CBL indicate (Fig. 5) that the surface heat flux anomaly may contribute to the deepening of the mixed layer, thus increasing the CBL height. However, the shear generated by the background wind strengthens the turbulent exchange between the entrainment layer and the free atmosphere, resulting in an excessively thick entrainment layer, which, however, inhibits the upward development of CBL.

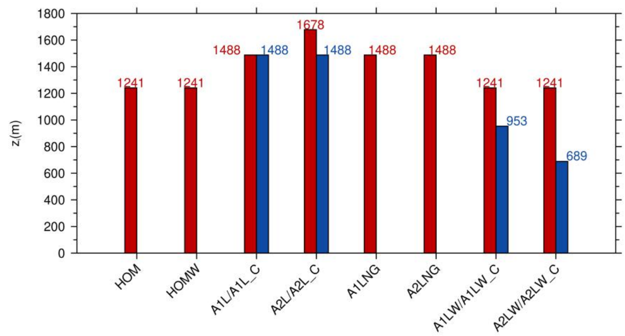


**Fig. 5.** Bar chart of the CBL height for each run marked with a concrete value. The red bars from left to right represent runs HOM, HOMW, A1L, A2L, A1LNG, A2LNG, A1LW, and A2LW. The blue bars from left to right represent runs A1L_C, A2L_C, A1LW_C, and A2LW_C.

### 3.2.2 Effects of the surface heat flux anomalies and background winds on the turbulent kinetic energy

Local circulations will be induced by differential heating, and the turbulent kinetic energy (TKE) determines the transport of the momentum, heat, and moisture through the boundary layer (Tyagi and Satyanarayana, 2013). Thus, the thermal circulations induced by the lake patches were simulated to investigate the effects of the heterogeneous heating on the spatial distribution of the TKE.

Fig. 6 shows the vertical distribution of the TKE and the wind vectors over the homogeneous and heterogeneous surfaces with no background wind at 15:30 LT. Over

https://doi.org/10.5194/acp-2021-325
Preprint. Discussion started: 9 July 2021


the homogeneous surface (Fig. 6a), a relatively uniform TKE with a larger magnitude exists within a much shallower CBL (below 0.1 *zi*), which overlies the scattered and disordered wind vectors throughout the domain. Over the heterogeneous surfaces, the large TKE values are distributed on both sides of the lake patches below 0.5 *zi*, and the divergent winds extend to about 30 km away. In addition, a larger TKE and convergent winds occurred in the upper level of the CBL (Figs. 6b, 6c). Moreover, the air flow between the two lake patches led to a convergent region (updrafts in y= 0 km; Fig. 6c). This is consistent with the results of Avissar and Schmidt (1998), who demonstrated that turbulent eddies are randomly distributed over a homogeneous surface, but the TKE exhibits two maxima near the ground surface and the top of the CBL, which is in agreement with the patch-induced circulations. Overall, Figure 6 illustrates that the distributions of the TKE and the patch-induced circulations are symmetrical on both sides of the lake patches, while the distribution is random with smaller TKE values over the homogeneous surface.

Furthermore, the ratios of the horizontally averaged TKEs in the model domain of the different runs were calculated to examine the effects of the surface anomalies and the ambient winds on the TKE. As is shown in Table 2, the TKEs for the cases with one or two lake patches are about twice that of the TKE of the case without patches (columns 2–3), but the ambient wind leads to a reduction in the impacts of surface flux heterogeneity on the TKE (columns 4–5 and 6–7). This is consistent with the results of Avissar and Schmidt (1998), who reported that a weak background wind of 2.5 m/s is strong enough to considerably reduce the impact of the ground-surface

https://doi.org/10.5194/acp-2021-325
Preprint. Discussion started: 9 July 2021



heterogeneity on the CBL. For the homogeneous cases, the TKE increases under the background wind conditions due to the increase in the sheared turbulence. For the runs with balanced surface heat fluxes (A1L_C, A2L_C, A1LW_C, A2LW_C), the effects of the heterogeneity on the TKE are less significant, especially for the cases with more lake patches, but the effects of the background winds on the TKE tend to be large.

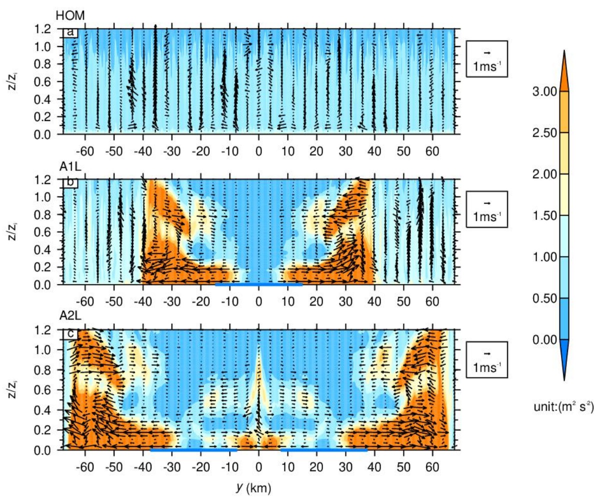


**Fig. 6.** The y-z cross sections of the TKE (contour) with superimposed wind vectors composed of *v* and *w* wind over (a) homogeneously heated and (b and c) heterogeneously heated surfaces. The blue lines on the y-axis represent the lake patches.

**Table 2**

The ratio of the TKEs of the different runs. Max, Min, and Mean stand for the maximum, minimum, and mean ratios of the TKE in the model domain, respectively.

| Ratio of TKE | A1L/HOM | A2L/HOM | A1LW/HOMW | A2LW/HOMW | A1LW/A1L | A2LW/A2L | HOMW/HOM |
|---|---|---|---|---|---|---|---|
| Max | 3.31 | 3.30 | 1.47 | 1.42 | 1.01 | 0.88 | 2.09 |
| Min | 1.15 | 1.18 | 0.80 | 0.59 | 0.61 | 0.40 | 0.83 |
| Mean | 2.00 | 2.04 | 1.09 | 0.95 | 0.79 | 0.68 | 1.41 |
| Ratio of TKE | A1L_C/HOM | A2L_C/HOM | A1LW_C/HOMW | A2LW_C/HOMW | A1LW_C/A1L_C | A2LW_C/A2L_C | HOMW/HOM |
| Max | 2.21 | 1.44 | 1.12 | 0.74 | 1.84 | 2.17 | 2.09 |
| Min | 0.43 | 0.23 | 0.63 | 0.31 | 0.80 | 0.47 | 0.83 |

https://doi.org/10.5194/acp-2021-325
Preprint. Discussion started: 9 July 2021




| | | | | | | | |
|---|---|---|---|---|---|---|---|
| Mean | 1.09 | 0.75 | 0.91 | 0.54 | 1.22 | 1.07 | 1.41 |

To further investigate the effects of the surface heat flux anomalies on the development of turbulence, it is instructive to examine the vertical profiles of the buoyancy and shear production terms in the TKE budget equation, which is from the contributions of the resolved (RES) and subgrid (SGS) eddies (Figs. 7a, 7b, and 7c).

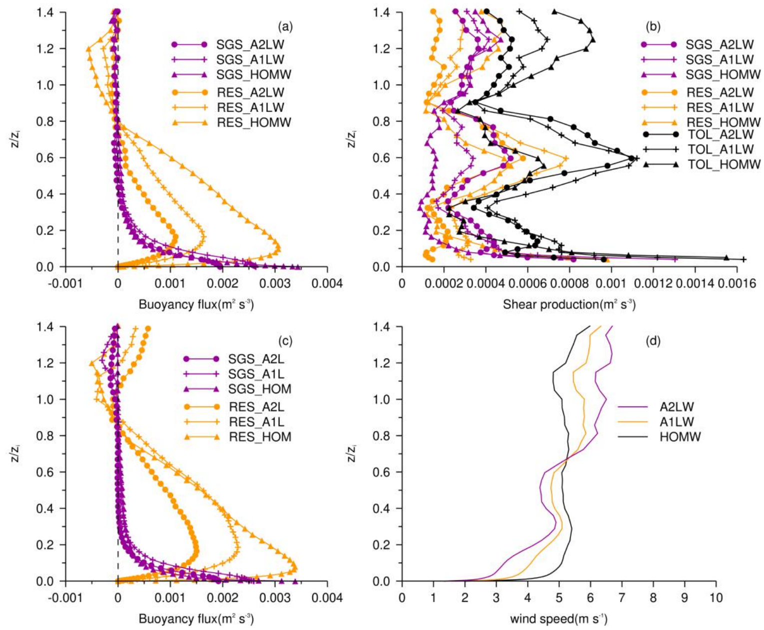


**Fig. 7.** Vertical profiles of (a) the buoyancy flux and (b) the shear production term for runs HOMW, A1LW, and A2LW with background flows, and (c) the profiles of the buoyancy flux for runs HOM, A1L, and A2L without background flows. (d) The simulated horizontal wind versus height for runs HOMW, A1LW, and A2LW. The resolved and subgrid results are presented as yellow and purple lines, respectively. The black lines in (b) are the total (resolved and subgrid scale) shear production term.

Figures 7a and 7c show that the RES buoyancy production decreases as the number of patches increases and the SGS buoyancy contributions are negligible, except in the surface layer. Below 0.9 *zi*, the larger RES shear production occurs in the case with lake patches (Fig. 7b) and the contribution of the SGS shear production is

https://doi.org/10.5194/acp-2021-325
Preprint. Discussion started: 9 July 2021




considerable (Fig. 7b), which is significant in the CBL for the cases with surface flux anomalies. Thus, the total shear productions (black lines in fig. 7b) of the cases with heterogeneous surfaces are larger. The background winds (Fig. 7d) are weaker for the cases with lake patches below 0.65 *zi,* but the corresponding total shear production term is larger, which shows that the patch-induced circulations are conducive to more shear in the CBL.

### 3.2.3 Effects of the background flows on the circulations

In order to investigate the effects of the background winds on the patch-induced circulations, the vertical distributions of the vertical velocity and wind fields for the runs with and without background winds were compared. In fig. 8, the patch-induced circulations are not easy to distinguish in the cases with background winds (about 13.9 m/s above a height of 1.2 km) due to the cancellation of the local pressure gradient by the synoptic pressure gradient, which is consistent with the results of Crosman and Horel (2010). This also indicates that the boundary-layer convection tends to weaken as the number of lake patches increases (the maximum updrafts are 4.8 m $s^{-1}$, 4.2 m $s^{-1}$, 3.5 m $s^{-1}$, and 3.3 m $s^{-1}$ for runs A1L, A2L, A1LW, and A2LW, respectively). Moreover, the wind fields for the cases without geostrophic winds exhibit divergent flows over the lake patches. As in the study of Kang and Lenschow (2014), our study also confirms that the symmetrical patch-induced circulations and the intensity of the convection become indistinguishable and weak under the background flow conditions. However, the divergent flows in the lower level are still visible when the geostrophic wind is removed (A1LNG and A2LNG in figs. 8e and

https://doi.org/10.5194/acp-2021-325
Preprint. Discussion started: 9 July 2021



8f).

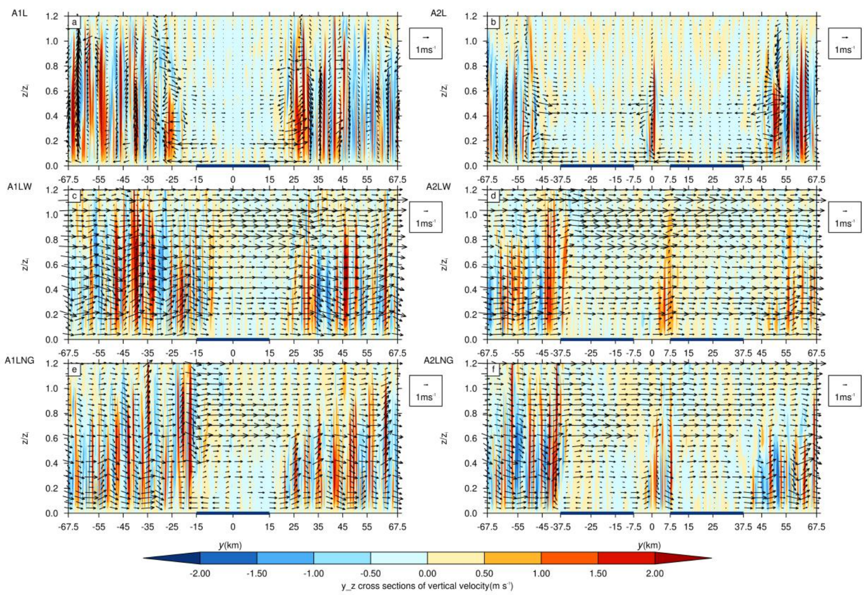


**Fig. 8.** Instantaneous y-z cross sections of the vertical velocity (m s$^{-1}$) and wind vectors above the heterogeneous surfaces for runs (a and b) without and (c and d) with background winds, and (e and f) with the geostrophic wind removed. The blue lines represent the lake patches.

## 3.3 Effects of patch-induced circulation on the turbulent intensity and heat flux

We used the phase-averaged method to decompose the contributions of the turbulent intensity and the heat flux from the patch-induced circulations and the background turbulence and to quantitatively analyze the heterogeneity-induced contribution to the turbulent intensity. For the variance of the velocity, the horizontal (Fig. 9a) and vertical (Fig. 9b) variances induced by the heterogeneity increase as the number of lake patches increases, and the horizontal variance is larger than the vertical variance. However, the background flows tend to decrease both the

https://doi.org/10.5194/acp-2021-325
Preprint. Discussion started: 9 July 2021


Atmospheric Chemistry and Physics
Open Access
Discussions

patch-induced (Figs. 9a, 9b) and total (Figs 9e, 9f) turbulent intensity.

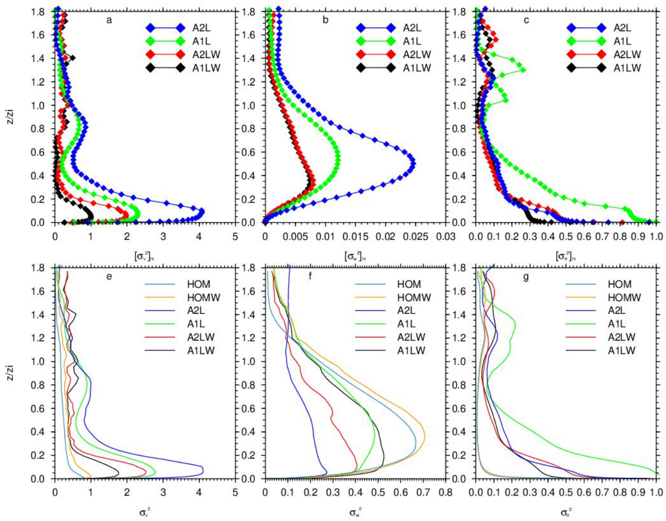


**Fig. 9.** (a, b, c) Heterogeneity-induced and (e, f, g) total dimensionless turbulence statistics for runs HOM, HOMW, A1L, A1LW, A2L, and A2LW. Shown are the profiles of the (a, e) *v* variance, (b, f) *w* variance, and (c, g) $\theta$ variance.

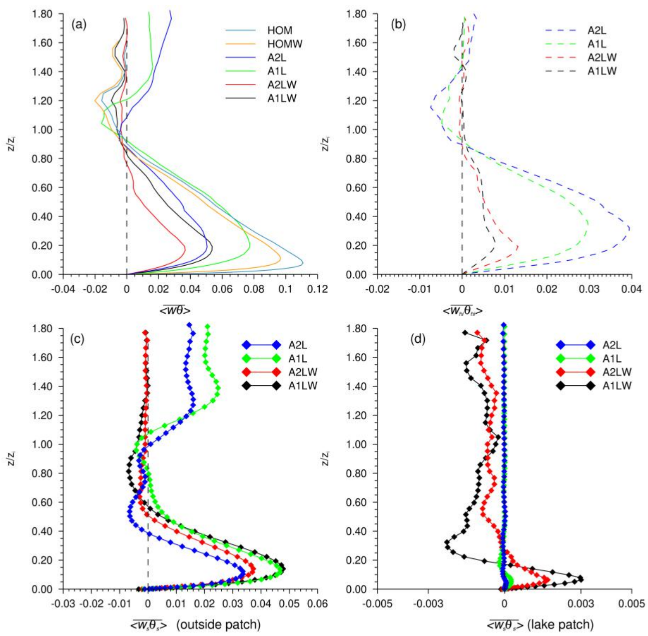


**Fig. 10.** (a) Area-averaged total turbulent heat flux (solid lines) and (b) heterogeneity-induced

https://doi.org/10.5194/acp-2021-325
Preprint. Discussion started: 9 July 2021




turbulent heat flux (dash lines). The background turbulence (lines with diamond symbols) of heat flux over the (c) grassland and (d) lake patches.

This also shows that a larger difference in the variances of the horizontal velocity occurs in the surface layer and gradually decreases with height (Figs. 9a and 9e), which means that the effects of the surface properties on the horizontal turbulence diminish with height in the CBL. In this respect, our results are similar to those found by Wang et al. (2011), Shao et al. (2013), and Frederik and Matthias (2018). The total horizontal turbulent intensity is mainly from the contribution of the patch-induced circulations and is larger than that of the homogeneous cases (Fig. 9e), which tends to become stronger as the number of patches increases but becomes weaker as the total vertical turbulent intensity increases (Fig. 9f, same as in the cases with balanced surface fluxes). It should be noted that the contribution of the patch-induced circulations to the vertical velocity variance is no more than 10% (Fig. 9b and 9f), which implies that the background turbulence contributes more to the fluctuations in the vertical velocity than to those in the horizontal velocity. Figures 9c and 9g show that the patch-induced motions make the largest contribution to the variances of the potential temperature. However, the background winds decrease the variances of the potential temperature and decrease the impact of the surface heterogeneity on the variances of the potential temperature.

Using the same method, we analyzed the contributions of the patch-induced and background turbulence to the heat flux. Figure 10a shows that as the number of lake patches increases, the area-averaged total heat flux decreases in both the mixed and

https://doi.org/10.5194/acp-2021-325
Preprint. Discussion started: 9 July 2021




entrainment layers, and the balanced surface heat flux cases exhibit similar variations (see fig.03 in supplement). The patch-induced transport of the heat flux increases as the number of lake patches increases (Fig. 10b). The patch-induced motions contribute up to 80% of the heat flux in run A2L, which has unbalanced surface fluxes (Fig. 10b), and 61% in run A2L_C which has balanced surface fluxes (see fig. S3 in supplement). It should also be noted that the background winds tend to decrease the heat flux transport over the heterogeneous surfaces. As is shown in figs. 10c and 10e, the contribution of the background turbulence to the local heat flux is larger over the region outside of the lake patches than over the patches. We hope that the results of our analysis of the contributions of the heterogeneity-induced circulation and background turbulence to the turbulence intensity and the heat flux over a heterogeneous surface will provide a basis for further studies of the local energy and mass transport in the SRYR over the TP.

## 3.4 Turbulence in the surface layer

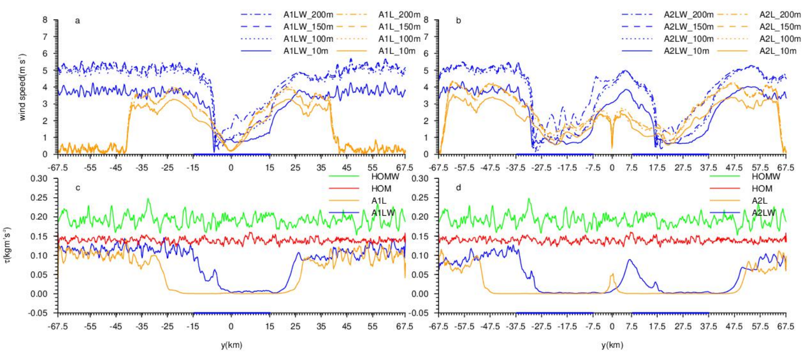


**Fig. 11.** Variations in the (a and b)wind speed and (c and d) Reynolds stress in the horizontal direction below 200 m for the cases with (blue lines) and without (yellow lines) background flows.

The frictional velocity ($u_*$) is a critical parameter in the turbulence exchange near the surface, and it plays an important role in the transport of momentum in the boundary layer. Patil et al. (2016) reported that the frictional velocity increases with increasing wind speed under lower wind speed conditions in the surface layer. Thus, we focused on the variations in the wind speed (Figs. 11a and 11b) and Reynolds stress (Figs. 11c and 11d) in the horizontal direction below 200 m in order to investigate the effects of the patch-induced motions on the momentum flux in the surface layer for various background winds. It was found that the inland extension of the patch-induced divergent flows reached about 25 km with no background winds (yellow curves in figs. 11a and 11b). The speed of the divergent winds increases from the lake patches to the outside and increases with height below 200 m with and without background winds. The wind speeds decrease rapidly (4.0 m $s^{-1}$) within 10 km along with the wind blowing from west of the lake patches to east of the lake patch, and then, the wind speeds increase steadily (blue curves in figs. 11a and 11b). The changes in the surface winds and surface properties have significant effects on the turbulent momentum flux. Figures 11c and 11d show that the transport of the momentum flux is smaller over the heterogeneous surface. The consistent variations in the wind speeds and the turbulent stresses illustrate that the lake patches alter the spatial distribution of the turbulent stress, which would further affect the surface wind speeds, especially over the land-lake boundary regions.

https://doi.org/10.5194/acp-2021-325
Preprint. Discussion started: 9 July 2021




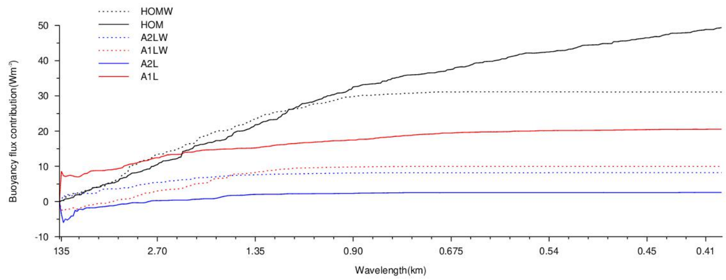


**Fig. 12.** The cumulative contribution of the buoyancy fluxes of all wavelengths (km) at a height of 50 m for runs HOM, HOMW, A1L, A2L, A1LW, and A2LW.

In order to quantify the contributions of the buoyancy fluxes, due to the different scales of the eddies, we calculated the ogives, which are the running integrals of the cospectral densities (Friehe et al., 1991), and used these values to show the cumulative contribution to the fluxes of all of the wavelengths (Brooks and Rogers, 2000). The ogive curves (Fig. 12) show that the small eddies make a significant contribution to the buoyancy fluxes over the homogeneous surfaces with no background winds (solid black line). The background wind increases the buoyancy flux for wavelengths larger than about 1.1 km and decreases it for smaller wavelengths based on a comparison of cases HOM (solid black line) and HOMW (black dotted line). The above results confirms that the heat transport is enhanced by the large eddies but is weakened by the small eddies, especially under the control of the background wind. The buoyancy flux for a wavelength larger than about 2.2 km makes a greater contribution in the case with one lake patch without background wind (solid red line). The buoyancy fluxes for wavelengths of greater than 2.7 km are transported downward for the case with two lake patches. For the case with one lake patch, the background flows tend to decrease the transport of the buoyancy flux for

https://doi.org/10.5194/acp-2021-325
Preprint. Discussion started: 9 July 2021



larger wavelengths near the surface (red dotted line) due to the stronger horizontal wind (Fig. 7d), and they help to transport the buoyancy fluxes downward for wavelengths larger than 3.3 km. However, for the case with two lake patches, the background wind causes the large eddies to transport the buoyancy fluxes upward. Thus, increasing the number of lake patches leads to more patch-induced motions, but this does not tend to enhance the ability of the wind to transport heat. It is concluded that slightly more of the buoyancy flux of the case with one lake patch is transported by the small eddies with wavelengths of less than 1.5 km compared with the case with two lake patches and background wind conditions (red and blue dotted lines).

### 3.5 The characteristics of the boundary-layer turbulence in the entrainment layer

The LES study conducted by Matthias et al. (2014) found that there is increased entrainment from the more strongly heated surface patch cases compared to the homogeneous cases, and the impact of the heterogeneity on entrainment vanishes due to horizontal mixing if the mean flow is aligned perpendicular to the border between the differentially heated patches. To investigate the effects of the thermal properties of the heterogeneous surface and the background flows on the turbulence in the entrainment layer, the characteristics of the heat flux in the entrainment layer were analyzed. Our simulated results show that the downward transport of the heat flux decreases as the number of lake patches increases in the entrainment layer for both the wind and no wind cases (Figs. 4d and 10a), which is also true in the balanced heat flux runs.

https://doi.org/10.5194/acp-2021-325
Preprint. Discussion started: 9 July 2021




By comparing the maximum and minimum vertical velocities at the top of the boundary layer (Table 3), we found that the convective intensity of the entrainment layer in the case with two lake patches and no wind fields is stronger, but it is weakened by the background flows. Whereas, it decreases as the number of lake patches increases in the balanced heat flux cases (A1L_C and A2L_C), corresponding to a smaller TKE (Table 2) and total turbulent intensity (Fig. 9f). Huang et al. (2007) pointed out that an appropriate surface heat flux and background flows maintain the convective roll, and our simulations demonstrate this roll-like convection (see fig. S4 in supplement), which is mainly induced by the persistence of the background turbulence with stronger geostrophic winds of 7–11 m $s^{-1}$ (black lines in fig. 2g). However, Maronga and Raasch (2013) found that a higher wind speed of 6 m $s^{-1}$ generates convective rolls derived from the secondary circulation over a complex heterogeneous surface.

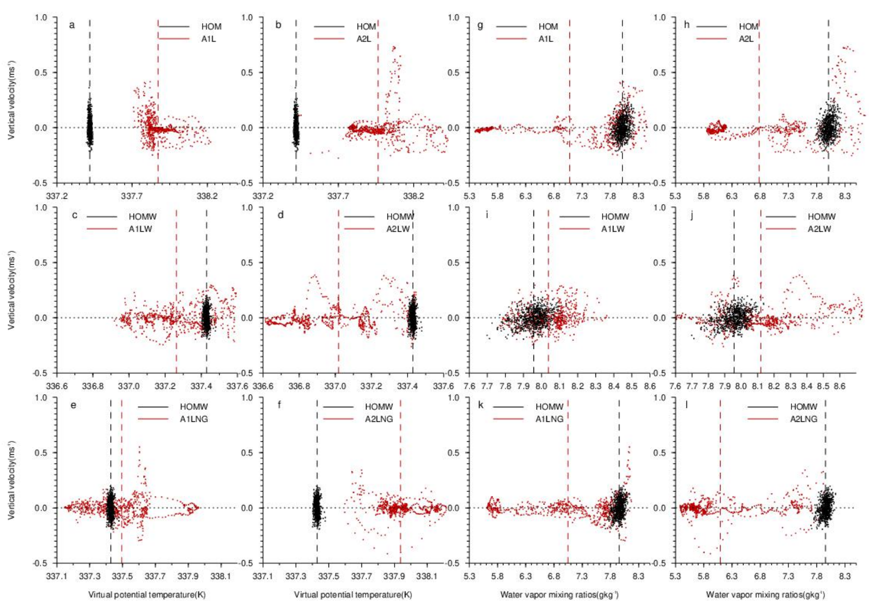

https://doi.org/10.5194/acp-2021-325
Preprint. Discussion started: 9 July 2021



**Fig. 13.** (a, b, c, d, e, f) The joint vertical velocities and virtual potential temperatures and (g, h, i, j, k, l) water vapor mixing ratios at the top of the CBL for the homogeneous and heterogeneous runs. The black dotted lines represent the mean vertical velocity, and the black and red dashed lines show the mean virtual potential temperatures and water vapor mixing ratios, respectively.

In addition, the boundary layer variables (including the vertical velocities, virtual potential temperatures, and water vapor mixing ratios) in the entrainment layer are also subject to the effects of the surface heterogeneity. Figure 13 shows the joint distribution of the vertical velocities and the virtual potential temperatures, as well as the vertical velocities and water vapor mixing ratios. Comparing to the homogeneously heated cases, the increased downdrafts mainly occur over the lake patches, and they carry more warm, dry air down from the free atmosphere (Figs. 13a, 13b, 13g, and 13h), which is due to the convergent airflow caused by the patch-induced circulations at the top of the CBL. This effect is much more evident in the case with two lake patches, but it is weakened by the gradually strengthening background flows (except figs. 13a, 13b, 13g, and 13h). We obtained the same results for the balanced cases. In particular, colder and moister air exists in the entrainment layer in the cases with ambient winds (A1LW_C and A2LW_C).

**Table 3**

The maximum and minimum vertical velocities at the top of the boundary layer in cases A1LW, A2LW, A1LW_C, A2LW_C, A1LNG, A2LNG, A1L, A2L and HOM, HOMW.

| Case | A1LW | A2LW | A1L | A2L | HOM | HOMW |
|---|---|---|---|---|---|---|
| W(max) | 4.01 | 3.54 | 5.42 | 5.55 | 4.37 | 4.48 |
| W(min) | −2.29 | −1.98 | −2.40 | −3.12 | −2.15 | −2.50 |
| Case | A1LW_C | A2LW_C | A1L_C | A2L_C | A1LNG | A2LNG |
| W(max) | 2.97 | 2.06 | 4.26 | 2.46 | 3.90 | 4.46 |
| W(min) | −2.03 | −1.25 | −1.91 | −1.27 | −2.23 | −1.97 |

https://doi.org/10.5194/acp-2021-325
Preprint. Discussion started: 9 July 2021

Atmospheric Chemistry and Physics
Discussions

## 4 Summary and discussion

The downdrafts and divergent zonal wind in the two lakes area obtained from the ERA-Interim reanalysis data indicate the existence of a lake breeze in the SRYR. Ten runs of the 1D strip-like distribution of the surface heat flux and two homogeneously heated runs based on the observations made during the summer of 2012 in the Ngoring Lake Basin were conducted in order to investigate the effects of the patch-induced circulations on the boundary-layer turbulence and its energy transport at the lake-air and grass-air interfaces, and the influence of the background flows also be considered.

The thermodynamic heterogeneity of the surface is conducive to deepening the mixed layer, thus increasing the CBL height and enhancing the TKE when there are no background flows. The background flows bring shear, resulting in an excessively thick entrainment layer, which inhibits the growth of CBL and reduce the effects of the heterogeneously heated surface on the TKE. The distribution of the TKE over the heterogeneously heated surface is consistent with the patch-induced circulations described by Avissar and Schmidt (1998). In addition, the surface heat anomaly and background winds have similar effects on the CBL in the cases with a balanced surface heat flux, but the enhanced effects on the TKE are far lower in the cases with an unbalanced surface heat flux. Thus, it is more beneficial to consider the ambient winds. By analyzing the buoyancy and shear production terms in the TKE budget equation and separating the contribution of the resolvable-scale (RES) and subgrid-scale (SGS) eddies, we found that the contributions of the wind shear to the

TKE from the SGS eddies are considerable in the CBL (below 0.9$zi$) over a heterogeneously heated surface. The total shear production term is larger below 0.65$zi$ in the heterogeneously heated cases with weaker background winds, demonstrating that the patch-induced circulations are conducive to producing more shear in the CBL. We obtained the same conclusion as Kang and Lenschow (2014), that is, the patch-induced circulations become indistinguishable under background flows conditions, and the ambient winds also weaken the convective intensity.

Then, we conducted a phase-averaged analysis to separate the contributions of the turbulent intensity and the transport of the total heat flux from those of the patch-induced circulations and the background turbulence field. The patch-induced turbulent intensity increases with increasing lake patches. It mainly contributes to the horizontal turbulent intensity and the potential temperature variance, while it contributes no more than 10% to the vertical turbulent intensity, of which the background turbulence contributes the most. The ambient winds weaken the patch-induced and horizontal turbulent intensities but strengthen the vertical turbulent intensity. The contribution of the patch-induced heat flux was up to 80% in the unbalanced cases and 60% in the balanced cases. The background turbulence made a larger contribution to the heat flux over the area outside of the patches, which have a stronger surface heat flux than that over the lake patches. The background flows also inhibit the transport of the heat flux.

To understand the effects of the patch-induced motions on the momentum flux in the surface layer under various background wind conditions, we focused on the

https://doi.org/10.5194/acp-2021-325
Preprint. Discussion started: 9 July 2021



variations in the wind speed and the Reynolds stress in the horizontal direction below 200 m. Without ambient winds, the inland extent of the patch-induced flows was about 25 km. When the background winds flowed into the lake patches, they decreased by 4.0 m $s^{-1}$ within about 10 km and increased steadily when flowing out of the patches. The synchronized variations in the wind speed and momentum flux in the horizontal direction illustrate that the lake patches alter the spatial distribution of the turbulent stress, which further affects the surface wind speeds, especially over the land-lake boundary regions. We also analyzed the cumulative contribution of eddies with different scales to the buoyancy flux near the surface. It was found that without background flows, the buoyancy flux is transmitted upward by the eddies with larger wavelengths for the case with one lake patch; while there is a negative buoyancy flux in the case with two lake patches. Thus, increasing the number of lake patches leads to more patch-induced motions, which do not tend to enhance the heat transport ability. The background flows promote the opposite results.

In the entrainment layer, in contrast to Matthias et al. (2014) who found that the entrainment increased for the stronger heated surface patch cases compared to the homogeneous case, we found that the entrainment flux decrease as the number of lake patches increases. For the unbalanced cases, the convective intensity increases as the number of lake patches increases, but the background flows weaken it. For the balanced cases, the convective intensity weakens as the number of lake patches increases, corresponding to a smaller TKE and total turbulent intensity. In this study, whether the convective rolls persist mainly depended on the background turbulence field with a higher geostrophic wind of 7–11 m s$^{-1}$, while Maronga and Raasch (2013) reported a higher wind speed of 6 m s$^{-1}$. As the number of lake patches increases, the increased downdrafts are mainly located over the lake patches, and they carry more warm, dry air down from the free atmosphere in both the balanced and unbalanced cases. The background winds weaken this effect even when there is cooler, moister air in the entrainment layer in the balanced cases.

Our study provides ideal simulations of the boundary-layer turbulence over the heterogeneously heated surface in the SRYR. It mainly focused on the influences of the heterogeneous distribution of the surface heat flux and the background winds. In the future, we plan to conduct further research that will take into consideration the topography and additional physical processes to provide a reference for the study of the energy and water exchange processes over the complex surface of the SRYR.

**Acknowledgments**

This research was supported by the second Tibetan Plateau Scientific Expedition and Research Program (STEP, 2019QZKK0604), the National Natural Science Foundation of China (NSFC) (91837208, 41775013). Thanks to the Zoige Plateau Wetland Ecosystem Research Station, Chinese Academy of Sciences for the field observation data, it supported by the Science and Technology Plan of Gansu Province (20JR10RA070).

**References**

Avissar, R., and Pielke, R. A.: A Parameterization of Heterogeneous Land Surfaces for Atmospheric Numerical Models and Its Impact on Regional Meteorology,

https://doi.org/10.5194/acp-2021-325
Preprint. Discussion started: 9 July 2021



Monthly Weather Review, 117(10), 2113-2136. doi:10.1175/1520-0493(1989)117<2113:APOHLS>2.0.CO;2, 1989.

Avissar, R., and Schmidt, T.: An Evaluation of the Scale at which Ground-Surface Heat Flux Patchiness Affects the Convective Boundary Layer Using Large-Eddy Simulations, Journal of the Atmospheric Sciences, 55(16), 2666 – 2689. doi:10.1175/1520-0469(1998)055<2666:AEOTSA>2.0.CO;2, 1998.

Ao, Y. H., Lyu, S. H., Li, Z. G., Wen, L. J., and Zhao, L.: Numerical simulation of the climate effect of high-altitude lakes on the Tibetan Plateau. Sciences in Cold and Arid Regions, 10(5): 0379 – 0391. doi: 10.3724/SP.J.1226.2018.00379, 2018.

Biermann, T., Babel, W., Ma, W. Q., Chen, X. L., Thiem, E., Ma, Y. M., and Foken, T.: Turbulent flux observations and modelling over a shallow lake and a wet grassland in the Nam Co basin, Tibetan Plateau. *Theor. Appli. Clima.*, **116**, 301-316, doi: 10.1007/s00704-013-0953-6, 2014.

Brierley, G. J., Li, X., Cullum, C. and Gao, C. (Eds.): Landscape and Ecosystem Diversity, Dynamics and Management in the Yellow River Source Zone, Springer International Publishing, 2016.

Brooks, I. M., and Rogers, D. P.: Aircraft observations of the mean and turbulent structure of a shallow boundary layer over the Persian Gulf [J]. Bound.-Layer Meteor., 95(2): 189 – 210. doi:10.1023/A:1002623712237, 2000.

Brown, A. R., Derbyshire, S. H. and Mason, P. J.: Large-eddy simulation of stable atmospheric boundary layers with a revised stochastic subgrid model. *Quart. J. Roy. Meteor. Soc.*, 120(520), 1485-1512,

https://doi.org/10.5194/acp-2021-325
Preprint. Discussion started: 9 July 2021


https://doi.org/10.1002/qj.49712052004, 1994.

Chen, X., Añel, J. A., Su, Z. B., Torre, L. D. L., Kelder, H., Peet, J. V., and Ma, Y. M., The Deep Atmospheric Boundary Layer and Its Significance to the Stratosphere and Troposphere Exchange over the Tibetan Plateau. *PLoS ONE,* **8**, e56909, https://doi.org/10.1371/journal.pone.0056909, 2013.

Chen, X., Škerlak, B., Rotach, M. W., Añel, J. A., Su, Z. B., Ma, Y. M., and Li, M. S.: Reasons for the extremely high-ranging planetary boundary layer over the western Tibetan Plateau in winter. *J. Atmos. Sci.*, **73**, 2021-2038, doi: 10.1175/JAS-D-15-0148.1, 2016.

Crosman, E. T., and Horel, J. D.: Sea and Lake Breezes: A Review of Numerical Studies. *Bound.-Layer Meteor.*, 137(1), 1－29. doi:10.1007/s10546-010-9517-9, 2010.

Crosman, E. T., and Horel, J. D.: Idealized Large-Eddy Simulations of Sea and Lake Breezes: Sensitivity to Lake Diameter, Heat Flux and Stability. *Bound.-Layer Meteor.*, **144**, 309-328, https://doi.org/10.1007/s10546-012-9721-x, 2012.

Friehe, C. A., Shaw, W. J., Rogers, D. P., Davidson, K. L., Large, W. G., Stage, S. A., Crescenti, G. H., Khalsa, S. J. S., Greenhut, G. K., and Li, F.: Air-sea fluxes and surface layer turbulence around a sea surface temperature front [J]. J. Geophys. Res., 96(C5): 8593－8609. doi:10.1029/90JC02062, 1991.

Foken, T., Matthias, M., Liebethal, C., Wimmer, F., Beyrich, F., Leps, J. P., Raasch, S., DeBruin, H. A. R., Meijninger, W. M. L., Bange, J.: Energy balance closure for the LITFASS-2003 experiment. Theor Appl Climatol., 101(1-2), 149-160.

doi:10.1007/s00704-009-0216-8, 2010.

Gray, M. E. B., Petch, J., Derbyshire, S. H., et al. 2001. Version 2.3 of the Met.Office large eddy model: part Ⅱ. Scientific documentation [R]. Met Office (APR) Turbulence and Diffusion Note No.276.

Hadfield, M. G., Cotton, W. R., and Pielke, R. A.: Large-eddy simulations of thermally forced circulations in the convective boundary layer. Part I: A small-scale circulation with zero wind. Boundary-Layer Meteorology, 57(1-2), 79-114. doi:10.1007/bf00119714, 1991.

Hadfield, M. G., Cotton, W. R., and Pielke, R. A.: Large-eddy simulations of thermally forced circulations in the convective boundary layer. Part II: The effect of changes in wavelength and wind speed. Boundary-Layer Meteorology, 58(4), 307-327. doi:10.1007/bf00120235, 1992.

Huang, Q., Marsham, J. H., Parker, D. J., Tian, W. S., Tammy, W.: A Comparison of Roll and Nonroll Convection and the Subsequent Deepening Moist Convection: An LEM Case Study Based on SCMS Data. Monthly Weather Review, 137(1), 350-365. doi:10.1175/2008MWR2450.1, 2009.

Jia, D., Wen, J., Ma, Y., Wang, X. and Lai, X.: The warm season characteristics of the turbulence structure and transfer of turbulent kinetic energy over alpine wetlands at the source of the yellow river. Meteorology & Atmospheric Physics, 130(1), 1-14. doi: 10.1007/s00703-017-0534-9, 2017.

Kang, S. L., and Lenschow, D. H.: Temporal evolution of low-level winds induced by two-dimensional mesoscale surface heat-flux heterogeneity. Boundary-Layer

https://doi.org/10.5194/acp-2021-325
Preprint. Discussion started: 9 July 2021


Meteorology, 151: 501－529. doi: 10.1007/s10546-014-9912-8, 2014.

Li, W. L., Lü, S. H., Fu, S. M., Meng, X. H., and Nnamchi, H. C.: Numerical simulation of fluxes generated by inhomogeneities of the underlying surface over the Jinta Oasis in Northwestern China. *Adv. Atmos. Sci*, **28**, 887-906, doi: 10.1007/s00376-010-0041-0, 2011.

Li, Z. G., Lyu, S. H., Ao, Y. H., Wen, L. J., Zhao, L., Wang, S. Y.: Long-term energy flux and radiation balance observations over Lake Ngoring, Tibetan Plateau. *Atmos. Res.*, **155**, 13-25, https://doi.org/10.1016/j.atmosres.2014.11.019, 2015.

Li, Z. G., Lyu, S. H., Wen, L. J., Zhao, L., Ao, Y. H., Wang, S. Y.: Effect of a cold, dry air incursion on atmospheric boundary layer processes over a high-altitude lake in the Tibetan Plateau. *Atmos. Res.*, **185**, 32-43, doi: 10.1016/j.atmosres.2016.10.024, 2017.

Liu, G., Sun, J. N., and Yin. L.: Turbulence characteristics of the shear-free convective boundary layer driven by heterogeneous surface heating. Boundary-Layer Meteorology, 140(1), 57-71. doi: 10.1007/s10546-011-9591-7, 2011.

Maronga, B., and Raasch, S.: Large-eddy simulations of surface heterogeneity effects on the convective boundary layer during the litfass-2003 experiment. Boundary-Layer Meteorology, 146(1), 17-44. doi: 10.1007/s10546-012-9748-z, 2013.

Marsham, J. H., Parker, D. J., Grams, C. M., Johnson, B. T., Grey, W. M. F., and Ross, A. N.: Observations of mesoscale and boundary-layer scale circulations affecting dust transport and uplift over the Sahara. *Atmos. Chem. Phys*, **8**,

https://doi.org/10.5194/acp-2021-325
Preprint. Discussion started: 9 July 2021



6979-6993, https://doi.org/10.5194/acp-8-6979-2008, 2008.

Matthias, S., Maronga, B., Florian, H., and Siegfried, R.: On the Effect of Surface Heat-Flux Heterogeneities on the Mixed-Layer-Top Entrainment. Boundary-Layer Meteorology, 151(3), 531-556. doi:10.1007/s10546-014-9913-7, 2014.

Moeng, C.-H.: A Large-Eddy-Simulation Model for the Study of Planetary Boundary-Layer Turbulence. *J. Atmos. Sci.*, **41**, 2052-2062, https://doi.org/10.1175/1520-0469(1984)041<2052:ALESMF>2.0.CO;2, 1984.

Mudassar, I., Wen, J., Wang, S. P., Tian, H., and Adnan, M.: Variations of precipitation characteristics during the period 1960-2014 in the source region of the Yellow River, China. Journal of Arid Land, 10(3): 388-401. https://doi.org/10.1007/s40333-018-0008-z, 2018.

Patil, M. N., Waghmare, R. T., Dharmaraj, T., Chinthalu, G. R., Devendraa, S., and Meena, G. S.: The influence of wind speed on surface layer stability and turbulent fluxes over southern Indian peninsula station. Journal of Earth System Science, 125(7), 1399–1411. doi:10.1007/s12040-016-0735-5, 2016.

Patton, E. G., Sullivan, P. P., and Moeng, C. H.: The influence of idealized heterogeneity on wet and dry planetary boundary layers coupled to the land surface. Journal of the Atmospheric Sciences, 62(7), 2078-2097. doi: 10.1175/JAS3465.1, 2005.

Shao, Y. P., Liu, S. F., Schween, J. H., and Crewell, S.: Large-Eddy Atmosphere-Land-Surface Modelling over Heterogeneous Surfaces: Model

https://doi.org/10.5194/acp-2021-325
Preprint. Discussion started: 9 July 2021



Development and Comparison with Measurements. Boundary-Layer Meteorology, 148(2), 333-356. doi: 10.1007/s10546-013-9823-0, 2013.

Shen, S. H., and Leclerc, M. Y.: How large must surface inhomogeneities be before they influence the convective boundary layer structure? A case study. Q. .I. R. Meteorol. soc., 121(526), 1209-1228. doi:10.1002/qj.49712152603, 1995.

Shen, L. D., Sun, J. N., Yuan, R. M., and Liu, P.: Characteristics of secondary circulations in the convective boundary layer over two-dimensional heterogeneous surfaces. *J. Meteor. Res.*, **30**, 944-960, https://doi.org/10.1007/s13351-016-6016-z, 2016.

Sommeria, G., and LeMone, M. A.: Direct testing of a three-dimensional model of the planetary boundary layer against experimental data. *J. Atmos. Sci.,* **35**, 25-39, https://doi.org/10.1175/1520-0469(1978)035<0025:DTOATD>2.0.CO;2, 1978.

Sullivan, P. P., Moeng, C., Stevens, B., Lenschow, D. H., and Mayor, S. D.: Structure of the Entrainment Zone Capping the Convective Atmospheric Boundary Layer, Journal of the Atmospheric Sciences, 55(19), 3042-3064. https://doi.org/10.1175/1520-0469(1998)055<3042:SOTEZC>2.0.CO;2, 1998.

Tyagi, B., and Satyanarayana, A. N. V.: The Budget of Turbulent Kinetic Energy during Premonsoon Season over Kharagpur as Revealed by STORM Experimental Data. *ISRN Meteorology*, **2013**, 1-11, doi: 10.1155/2013/972942, 2013.

Wang, B. B., Ma, Y. M., Chen, X. L., Ma, W. Q., Su, Z. B., and Menenti, M.: Observation and simulation of lake－air heat and water transfer processes in a

https://doi.org/10.5194/acp-2021-325
Preprint. Discussion started: 9 July 2021



high-altitude shallow lake on the Tibetan Plateau [J]. J. Geophys. Res., 120(24): 12327-12344. doi:10.1002/2015JD023863, 2015.

Wang, C., Tian, W. S., Parker, D. J., Marsham, J. H. and Guo, Z.: Properties of a simulated convective boundary layer over inhomogeneous vegetation. *Quart. J. Roy. Meteor. Soc*., **137**, 99-117, https://doi.org/10.1002/qj.724, 2011.

Wang, Y., Xu, X., Liu, H., et al., Wang, Y. J., Xu, X. D., Liu, H. Z., Li, Y. Q., Li, Y. H., Hu, Z. Y., Gao, X. Q., Ma, Y. M., Sun, J. H., Lenschow, D. H., Zhong, S. Y., Zhou, M. Y., Bian, X. D., and Zhao, P.: Analysis of land surface parameters and turbulence characteristics over the Tibetan Plateau and surrounding region. *J. Geophys. Res.: Atmospheres*, **121**, 9540-9560, doi:10.1002/2016JD025401, 2016.

Wen, L. J., Lyu, S. H., Li, Z. G., Zhao, L., and Nagabhatla, N.: Impacts of the Two Biggest Lakes on Local Temperature and Precipitation in the Yellow River Source Region of the Tibetan Plateau. *Adv. Meteor.*, **2015**, 10, doi:10.1155/2015/248031, 2015.

Wen, L. J., Lyu, S. H., Kirillin, G., Li, Z. G., and Zhao, L.: Air-lake boundary layer and performance of a simple lake parameterization scheme over the Tibetan highlands, Tellus A: Dynamic Meteorology and Oceanography, 68:1, 31091. doi: 10.3402/tellusa.v68.31091, 2016.

Xu, Z. W., Ma, Y. F., Liu, S. M., Shi, W. J., Wang, J. M.: Assessment of the Energy balance closure under advective conditions and its impact using remote sensing data. Journal of Applied Meteorology and Climatology, 56(1). doi:10.1175/JAMC-D-16-0096.1, 2016.

https://doi.org/10.5194/acp-2021-325
Preprint. Discussion started: 9 July 2021



Zhang, W. C., Guo, J. P., Miao, Y. C., Liu, H., Song, Y., Fang, Z., He, J., Lou, M. Y., Yan, Y., Li, Y., and Zhai, P. M.: On the summertime planetary boundary layer with different thermodynamic stability in China: A radiosonde perspective [J]. J. Climate, 31(4): 1451-1465. doi:10.1175/JCLI-D-17-0231.1, 2018.

Zhao, Y., Xu, X. D., Ruan, Z., Chen, B., and Wang, F.: Precursory strong-signal characteristics of the convective clouds of the Central Tibetan Plateau detected by radar echoes with respect to the evolutionary processes of an eastward-moving heavy rainstorm belt in the Yangtze River Basin. *Meteor. Atmos. Phys.,* 1-16, https://doi.org/10.1007/s00703-018-0597-2, 2018.

Zheng, D. H., Velde, R. V. D., Su, Z. B., Wang, X., Wen, J., Booij, M. J., Hoekstra, A. Y., and Chen, Y. Y.: Augmentations to the Noah Model Physics for Application to the Yellow River Source Area. Part II: Turbulent Heat Fluxes and Soil Heat Transport. *J. Hydromete.*, **16**, 2677-2694, https://doi.org/10.1175/JHM-D-14-0199.1, 2015.

Zhou, Y., Li. D., Liu, H. and Li, X.: Diurnal variations of the flux imbalance over homogeneous and heterogeneous landscapes. Boundary-Layer Meteorology, 168:417－442. https://doi.org/10.1007/s10546-018-0358-2, 2018.